Black Phosphorus–Monolayer MoS_2 van der Waals Heterojunction p–n Diode

Yexin Deng,[†,*] Zhe Luo,[§] Nathan J. Conrad,[†] Han Liu,[†] Yongji Gong,[‡] Sina Najmaei,[‡] Pulickel M. Ajayan,[‡] Jun Lou,[‡] Xianfan Xu,[§,*] and Peide D. Ye[†,*]

[†]School of Electrical and Computer Engineering and Birck Nanotechnology Center and [§]School of Mechanical Engineering and Birck Nanotechnology Center, Purdue University, West Lafayette, Indiana 47907, United States and [‡]Department of Mechanical Engineering and Materials Science, Rice University, Houston, Texas 77005, United States

ABSTRACT Phosphorene, a elemental 2D material, which is the monolayer of black phosphorus, has been mechanically exfoliated recently. In its bulk form, black phosphorus shows high carrier mobility (~10 000 $cm^2/V\cdot s$) and a ~0.3 eV direct band gap. Well-behaved p-type field-effect transistors with mobilities of up to 1000 $cm^2/V\cdot s$, as well as phototransistors, have been demonstrated on few-layer black phosphorus, showing its promise for electronics and optoelectronics applications due to its high hole mobility and thickness-dependent direct band gap. However, p–n junctions, the basic building blocks of modern electronic and optoelectronic devices, have not yet been realized based on black phosphorus. In this paper, we demonstrate a gate-tunable p–n diode based on a p-type black phosphorus/n-type monolayer MoS_2 van der Waals p–n heterojunction. Upon illumination, these ultrathin p–n diodes show a maximum photodetection responsivity of 418 mA/W at the wavelength of 633 nm and photovoltaic energy conversion with an external quantum efficiency of 0.3%. These p–n diodes show promise for broad-band photodetection and solar energy harvesting.

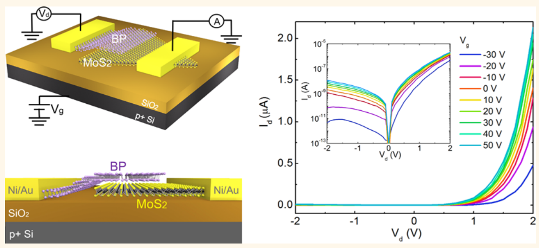

KEYWORDS: black phosphorus · phosphorene · MoS_2 · p–n diode · van der Waals heterojunction · photodetection · solar cell

The successful isolation of graphene from graphite has led to its extensive study in physics, materials, and nanoengineering due to its extraordinary electrical and mechanical properties.[1–4] However, a lack of a band gap limits its potential for electronic device applications and has inspired the exploration of other 2D-layered materials.[5–7] Among them, transition metal dichalcogenides (TMDCs), such as MoS_2, are the most studied materials.[8–11] Recently, phosphorene, the monolayer form of black phosphorus, has been successfully isolated.[12] Analogous to graphite and graphene, black phosphorus is a stack of phosphorene monolayers, bound together by van der Waals interactions.[12,13] Bulk black phosphorus shows a ~0.3 eV direct band gap and a mobility of up to ~10 000 $cm^2/V\cdot s$.[14–17] Its band gap increases as its thickness decreases and is predicted to have a >1 eV direct band gap in its monolayer form.[12,13] Well-behaved p-type field-effect transistors with mobilities of up to 1000 $cm^2/V\cdot s$, as well as inverters, have been demonstrated on few-layer black phosphorus.[12,13,18–20] Based on its direct band gap, few-layer black phosphorus phototransistors have been demonstrated with a responsivity of 4.8 mA/W.[19] These results indicate that black phosphorus is a promising candidate for both high-performance electronics and optoelectronics applications due to its ultrathin 2D nature, high hole mobility, and narrower direct band gap compared to most of TMDCs.

The p–n junctions are the basic building blocks of modern semiconductor devices, including diodes, bipolar transistors, photodiodes, light-emitting diodes, and solar cells. In the conventional p–n homojunction, the p- and n-type regions are formed by chemically doping a bulk semiconductor, creating a graded junction region. The p–n heterojunctions can be realized by epitaxially growing an n-type semiconductor on another p-type semiconductor or *vice versa* and can form abrupt p–n junctions. Relying on the van der Waals interactions, atomically

* Address correspondence to deng58@purdue.edu, xxu@purdue.edu, yep@purdue.edu.

Received for review May 19, 2014 and accepted July 14, 2014.

Published online July 14, 2014
10.1021/nn5027388

© 2014 American Chemical Society

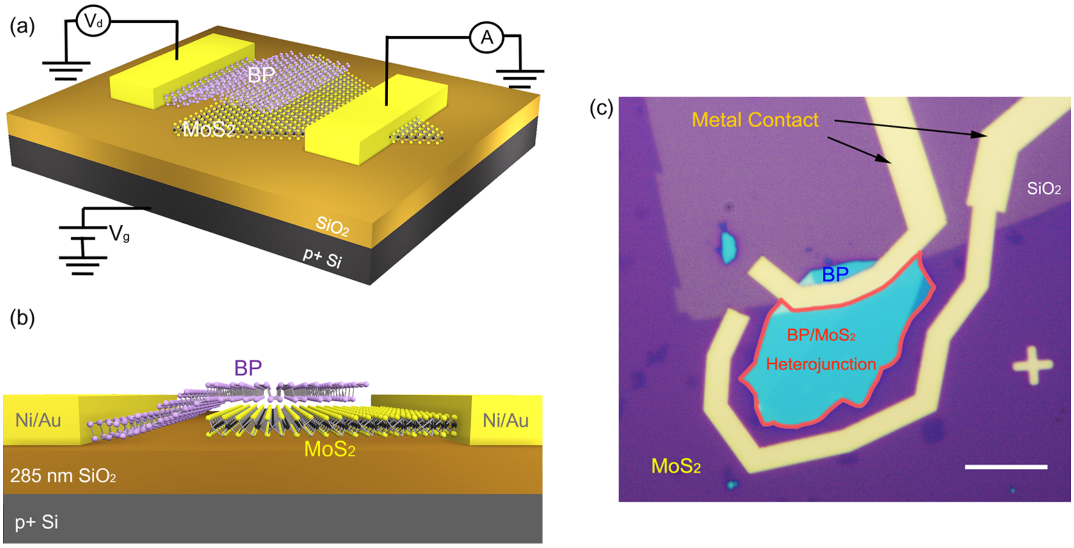

Figure 1. (a,b) Schematics of the device structure. A p+ silicon wafer capped with 285 nm SiO_2 is used as the global back gate and the gate dielectric. Few-layer black phosphorus flakes were exfoliated onto monolayer MoS_2 in order to form a van der Waals heterojunction. Ni/Au were deposited as contacts. During the electrical measurements, a voltage V_d is applied across the device. The voltage bias V_g is applied to the back gate. (c) Optical image of the fabricated device. The dark purple region is monolayer MoS_2, while the blue flake is few-layer black phosphorus. The light purple region is SiO_2. Scale bar, 10 μm.

sharp 2D heterostructures can be achieved without the problems caused by lattice mismatches between materials. Moreover, the ultrathin nature of 2D heterostructures allows for electrical modulation of the band structure in the vertical direction. This creates a new avenue for the realization of novel 2D electronic and optoelectronic devices.[21−33]

Here, we report an electrically tunable black phosphorus−monolayer MoS_2 van der Waals heterojunction p−n diode. To the best of our knowledge, this is the first 2D heterostructure demonstrated using black phosphorus. The p-type black phosphorus and n-type monolayer MoS_2 form an atomically sharp type II heterointerface through van der Waals interactions.[13,34] The p−n diode exhibits gate-tunable current-rectifying characteristics. Upon illumination, the p−n diode can be used as photodetector with a maximum responsivity of 418 mA/W, which is nearly 100 times higher than that reported for few-layer black phosphorus phototransistors and 26 times higher than that recently reported for WSe_2 p−n diodes.[19,35,36] The photovoltaic power generation in the diode reaches a peak external quantum efficiency of ~0.3%. Furthermore, photocurrent mapping confirms that the current is generated throughout the entire overlapped p−n junction region, showing its feasibility for use in large area solar cells and photodetectors.

RESULTS AND DISCUSSION

In the experiments, monolayer MoS_2 was synthesized by chemical vapor deposition (CVD) on a 285 nm SiO_2/p+-doped Si substrate using MoO_3 and sulfur. More information about the synthesis method can be found in our previous papers.[37,38] Few-layer black phosphorus was mechanically exfoliated using adhesive tape from bulk material onto a SiO_2 substrate on which CVD monolayer MoS_2 had been synthesized. Due to van der Waals interactions, 2D black phosphorus−monolayer MoS_2 heterojunctions can be formed at the overlapped regions. Electron-beam lithography was used to define the contact patterns. Finally, 20/60 nm of Ni/Au were deposited as metal contacts. Figure 1a,b shows the schematics of the device structure and the electrical connections. A voltage (V_d) was applied across the diode, and a voltage (V_g) was applied to the p+-doped silicon as a back gate, which can electrically modulate the device. The optical image of the fabricated device is shown in Figure 1c, and all the following results were obtained from this particular device unless otherwise specified. To achieve better current collection and reduce series resistance, the MoS_2 electrode is designed to surround the black phosphorus flake.

The thicknesses of the few-layer black phosphorus flake and monolayer MoS_2 are ~11 and ~0.9 nm, respectively, as determined from the atomic force microscopy measurements shown in Figure 2a. The monolayer nature of the MoS_2 can be further confirmed by the peak position (~1.8 eV) in its photoluminescence spectrum, shown in Figure 2b.[39] The Raman spectra from the black phosphorus, monolayer MoS_2, and the heterojunction regions are presented in Figure 2c. The observed Raman-active modes of black phosphorus and MoS_2 are consistent with previously reported data[12,37] The peaks of both MoS_2 and black phosphorus can be observed in the overlapped region with very little shift from their positions in the non-overlapped regions, indicating good quality of thin

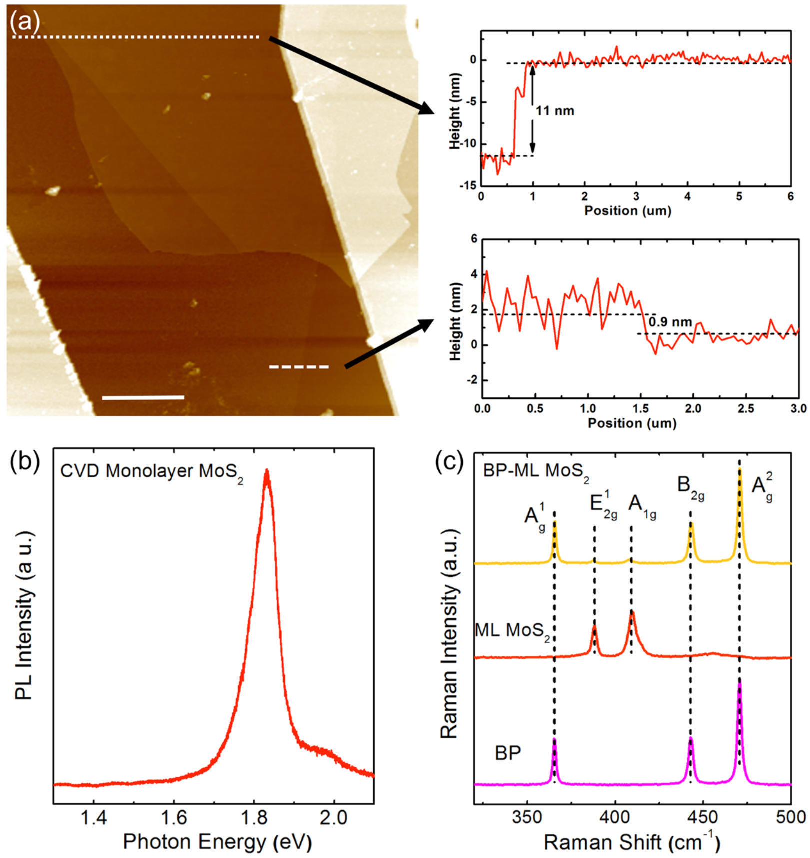

Figure 2. (a) Atomic force microscopy image of part of the junction region. It shows that the black phosphorus and MoS_2 films are ~11 and ~0.9 nm thick, respectively. Scale bar, 2 μm. (b) Photoluminescence spectrum of the MoS_2 thin film. It shows a strong peak close to 1.8 eV, confirming that the MoS_2 is a monolayer. (c) Raman spectra of the MoS_2, black phosphorus, and the overlapped regions. Both of the black phosphorus and MoS_2 Raman peaks can be observed in the overlapped region.

films in the junction region after exfoliation and device fabrication.

Next, we studied the electrical characteristics of the fabricated device. In this paper, all the measurements were performed in ambient atmosphere. Figure 3a shows the gate-tunable *I*−*V* characteristics of the p−n diode, and the inset (1) shows the *I*−*V* curves on a semilog plot. The current-rectifying characteristics can be modulated by the back gate voltage, shown in the inset (2) of Figure 3a. The rectification ratio, defined as the ratio of the forward/reverse current, increases as the back gate voltage decreases. By using −30 V back gate voltage, a rectification ratio of $\sim 10^5$ is obtained at $V_d = -2/+2$ V. Additionally, the ideal factor of the p−n diode increases as the back gate voltage increases (Supporting Information Figure S8) and achieves a minimum value of 2.7 with a back gate voltage of −30 V. These strong current-rectifying characteristics indicate that a good van der Waals p−n heterojunction formed between p-type black phosphorus and n-type MoS_2. The modulation effect of the back gate voltage can also be seen in the transfer curves (Figure 3b). Both forward and reverse currents can be substantially increased by increasing the back gate voltage. These results can be explained by a simplified model describing the current transport of the p−n diode (see Supporting Information for more details). For simplicity, the total resistance of the device can be roughly divided into three parts: the resistance of the p−n junction near the interface, the sheet resistances of MoS_2 and few-layer black phosphorus, and the contact resistances of metal/MoS_2 and metal/black phosphorus. The current-rectifying characteristics come from the p−n interface region, which may be modeled as many parallel p−n diodes (Figure S2a). The band alignment of MoS_2 and black phosphorus at the p−n junction interface can be modulated by the back gate voltage, as shown in Figure S3. This can explain why the rectification ratio increases as the back gate voltage decreases, and the ideal factor decreases as the back gate voltage decreases. Moreover, the back gate voltage can also modulate the sheet resistance and the contact resistance. As the device size is relatively large, the sheet resistances are more significant than the contact resistances. Because the sheet resistance of CVD monolayer MoS_2 is much larger than the 11 nm black phosphorus, the overall device resistance is strongly impacted by the resistance of MoS_2.[12,40] By increasing the back gate voltage (V_g), both the resistance of MoS_2 and its contact resistance are reduced,

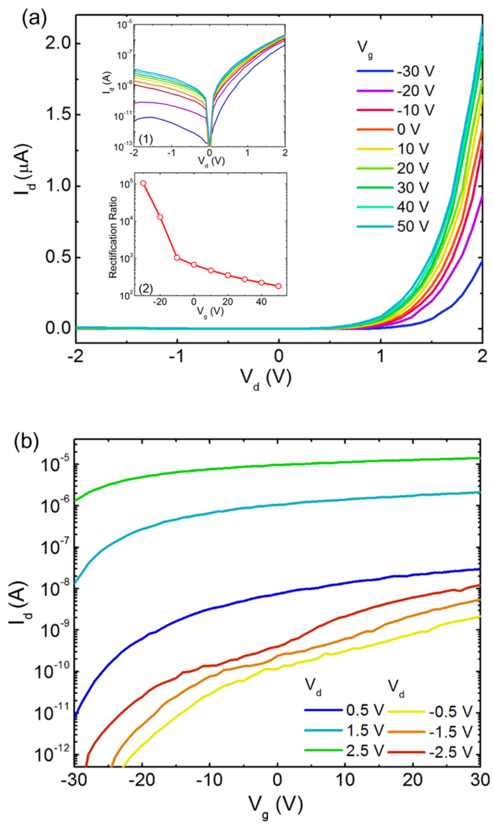

Figure 3. (a) Gate tunable *I*−*V* characteristics of the 2D p−n diode. The current increases as the back gate voltage increases. The inset (1) shows the *I*−*V* characteristics under semilog scale. The inset (2) shows the rectification ratio as a function of back gate voltage V_g. (b) Transfer curves of p−n diode for both forward and reverse V_d bias with back gate modulations.

which can efficiently boost the total current under both forward and reverse bias (see the Supporting Information for more details).

As good current-rectifying characteristics were achieved, the optoelectronic characteristics of these 2D p−n diodes were then explored. A 633 nm He−Ne laser was used to illuminate the device. The spot size of the laser was controlled to be much smaller than the junction area in order to exclude the photoresponse from the non-overlapped region. Figure 4a shows the *I*−*V* curves of the p−n diode under various incident laser power, and the inset shows the details of the negative V_d bias region. The photocurrent I_{ph} is defined as $I_{illumination} - I_{dark}$, where $I_{illumination}$ and I_{dark} are the I_d with and without laser illumination. Under reverse bias, the photocurrent has a strong dependence on the incident power (Figure 4b). By increasing the back gate voltage, the photocurrent is substantially increased. This can be attributed to the reduction of the MoS_2 sheet resistance and the MoS_2/metal contact resistance (see Supporting Information for more information). On the other hand, by applying a strong negative back gate voltage (−40 V) to modulate the band alignment of MoS_2 and black phosphorus (Figure S3), the ratio of the illumination current over the dark current ($I_{illumination}/I_{dark}$) can be increased to 3×10^3, though the illumination current decreases due to the increasing of sheet and contact resistance (see Supporting Information for more details). This is ∼100 times larger than that of a MoS_2 photodetector due to a better suppression of I_{dark} by the reversed bias p−n diode. Compared with the phototransistor, it is beneficial for the device to detect signal from noise.[41] With these results, the photodetection responsivity, *R*, defined as I_{ph}/P_{laser}, where P_{laser} is the incident power of the laser, can be calculated for both forward (as photoconductor) and reverse bias (as photodiode) as shown in Figure 4c. The responsivity of both the forward and the reverse bias regions decreases as the laser power increases, which is due to the saturation of electron−hole pair generation at higher incident light intensity and the increased surface recombination in either the junction region or the underlying SiO_2.[41] Therefore, to further improve the responsivity, it is necessary to improve the film quality of the CVD MoS_2 and black phosphorus, as well as the dielectric interface quality. In this device, the responsivity reaches 1.27 A/W and 11 mA/W for forward and reverse bias, respectively. The maximum responsivity in our devices is up to 3.54 A/W (at $V_d = +2$ V) and 418 mA/W (at $V_d = -2$ V) under 1 μW laser power (Figure S5). As a photodiode, this is nearly 100 times higher than that of the recently reported black phosphorus phototransistor and 4.8 times higher than that of the carbon nanotube−MoS_2 p−n diode with a much smaller V_d.[19,32] By using this electrically tunable 2D p−n diode, it is possible to realize sensitive and broad-band photodetection due to the high mobility and relatively small direct band gap of few-layer black phosphorus.

In addition to the photodetection, this p−n diode is also usable for photovoltaic energy conversion. Under laser illumination, the short circuit current (I_{sc}), which is the current through the device with 0 V bias, is shown in Figure 5a. The open circuit voltage (V_{oc}) can be obtained by examining the V_d axis intercepts in the plot. As seen in Figure 5c,d, both the I_{sc} and V_{oc} increase as the laser power increases. However, the back gate modulates the I_{sc} and V_{oc} in different ways. Increasing the back gate voltage boosts the I_{sc} while reducing the V_{oc}. This can be attributed to the opposite modulation effect of band alignment of MoS_2/black phosphorus at the junction interface and the sheet and contact resistance of MoS_2 (see Supporting Information for details). With these data, the power generated by the p−n diode can be calculated by $P_d = I_d V_d$, as shown in Figure 5b. Then, the fill factor, which is defined as $FF = P_d/(I_{sc}V_{oc})$, can be obtained. The maximum FF is ∼0.5 in this 2D p−n diode. Furthermore, the external quantum efficiency (EQE) can be calculated by $EQE = (I_{sc}/P_{laser})(hc/e\lambda)$, where *h* is the Planck constant, *e* is the electron charge, *c* is the velocity of light, and λ is the

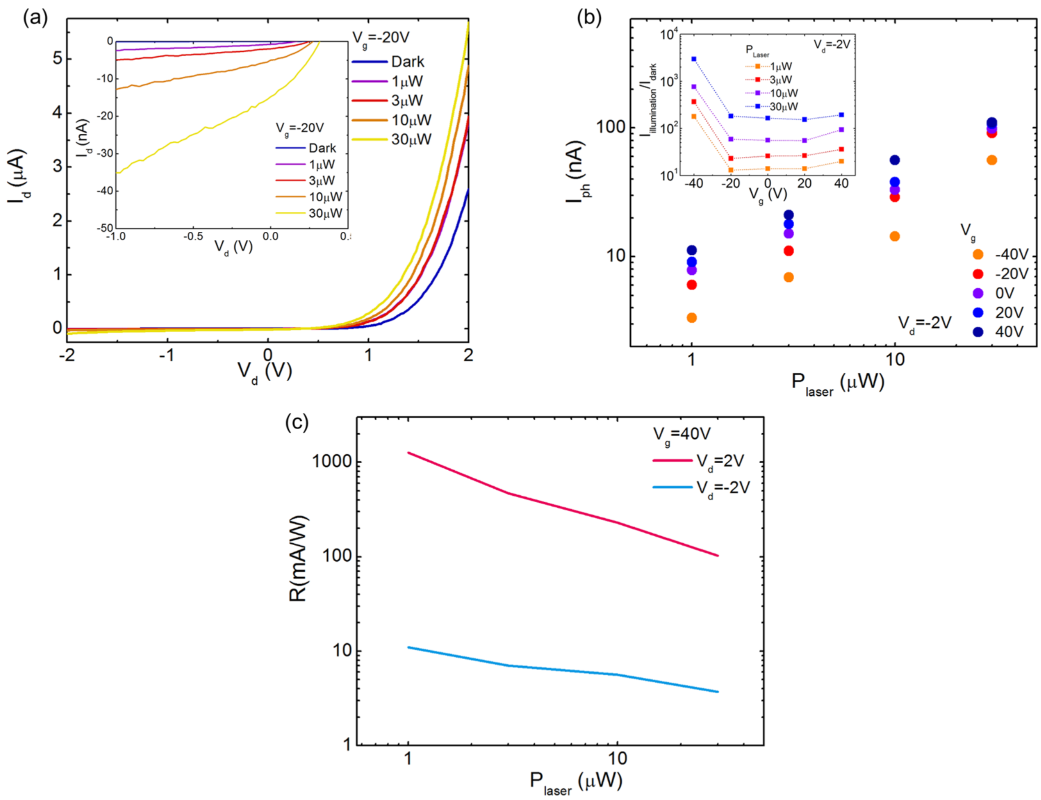

Figure 4. (a) *I*−*V* characteristics of the p−n diode under various incident laser powers. The inset shows the details in the reverse bias region. (b) Photocurrent as a function of incident laser power. Increasing the back gate voltage can increase the photocurrent. The inset shows the ratio of $I_{illumination}/I_{dark}$. (c) Photodetection responsivity (*R*) calculated as a function of incident power. The responsivity decreases as the power increases.

wavelength of the incident light. The peak EQE in this device is 0.3%. To the best of our knowledge, this is the first time that efficient photovoltaic energy conversion has been demonstrated using black phosphorus. By further reducing the thickness of the black phosphorus to bilayer, it is possible to essentially enhance the EQE to up to 18%, according to theoretical predictions.[42] Moreover, by stacking the 2D p−n diode vertically, a stacked solar cell structure can be realized. Since the direct band gap of black phosphorus changes with its thicknesses, the efficiency may be further improved by tuning its thickness to better utilize the photon energies of different wavelengths of the solar spectrum.[12]

To further understand the photoresponse process, photocurrent mapping was performed in order to determine the spatial distribution of the photocurrent generation. A device with a larger junction region was chosen to get more spatial information, as shown in Figure 6a. The thickness of the black phosphorus flake is ∼22 nm (Figure S6). A 633 nm He−Ne laser was used with ∼8 μW power and ∼1 μm spot size. The current was measured under 0 V bias. As seen in the Figure 6b, the current is generated throughout the junction region, which indicates the charge separation mainly in the heterojunction region. However, the photoresponse across the junction is not uniform. This can be attributed to the non-uniform contacts between the two flakes. Moreover, the part of the junction region that is near the metal contact on the MoS_2 exhibits stronger photocurrent. This is related to the lateral sheet resistance of MoS_2 and black phosphorus. Under illumination, the charges are separated near the vertical interface p−n diode region. For simplicity, we treat the interface p−n diode (see Figure S4) at a certain position as a voltage source under illumination. Here we assume the value of this voltage source is uniform across the junction if different positions are under laser illumination. The photocurrent flows though MoS_2 and black phosphorus to reach the metal contact (Figure S4). Because the sheet resistance of CVD monolayer MoS_2 is much larger than the black phosphorus, the resistance of the MoS_2 makes a much stronger impact. The part of the junction region closer to the metal contact (B in Figure S4, compared with A) on MoS_2 shows a lower MoS_2 sheet resistance, resulting in the stronger photocurrent near the contact of MoS_2 (see Supporting Information for details). To get a more uniform spatial photoresponse, a transparent contact material, such as graphene, could be used as top electrodes. This can increase the contact area and yield better carrier collection. Furthermore, graphene can also reduce the contact resistance as an interlayer between the metals and the TMDCs, further improving the device efficiency.[43] This scheme makes it possible for the black

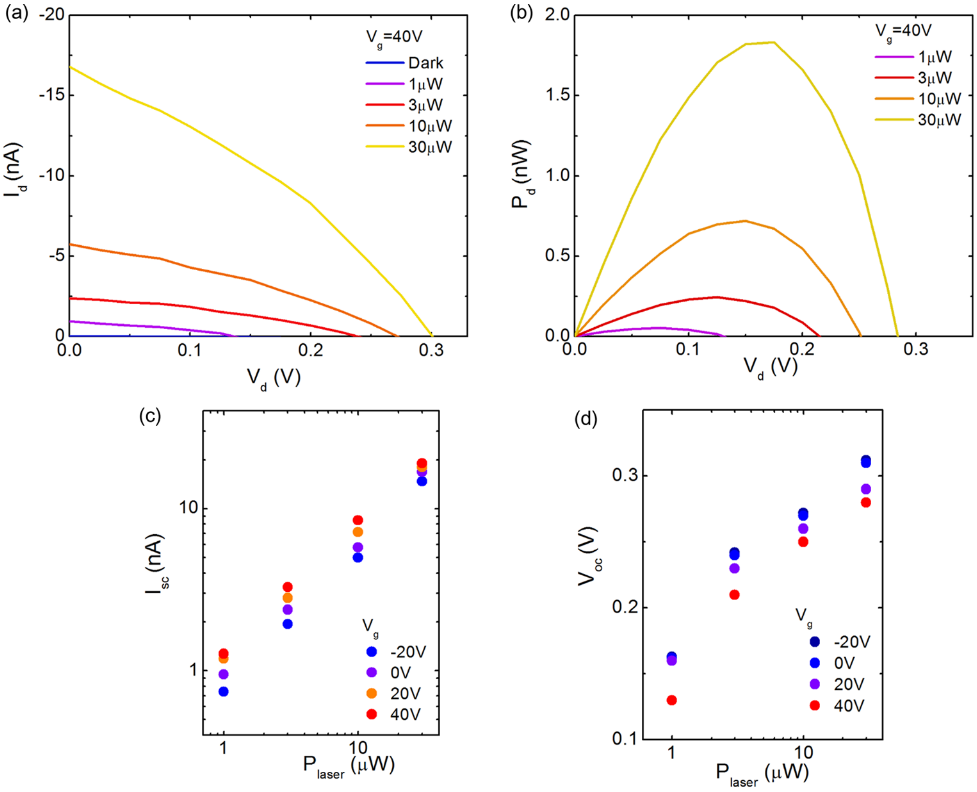

Figure 5. (a) I_d as a function of function of V_d under various laser powers. The I_{sc} and V_{oc} can be obtained from the intercepts of the curves on I_d and V_d axes. (b) Power generated by the p−n diode as a function of V_d under different laser power. (c) I_{sc} as a function of laser power under different back gate voltage. (d) V_{oc} as a function of laser power under different back gate voltage. Increasing the back gate voltage increases I_{sc} but reduces V_{oc}.

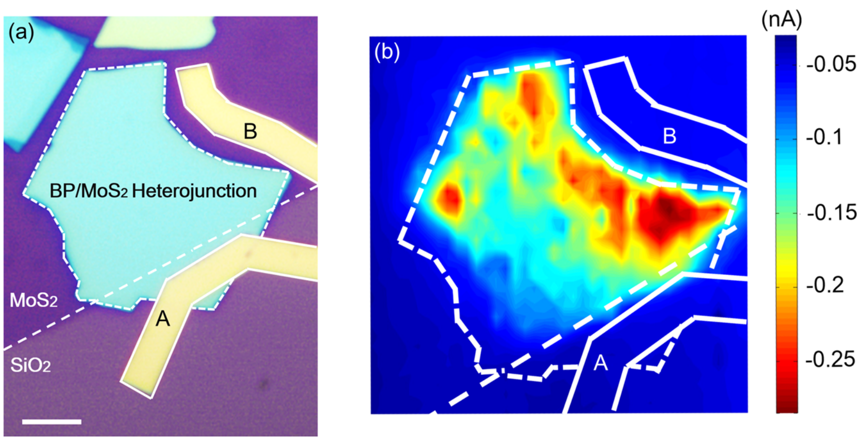

Figure 6. (a) Optical image of the p−n heterojunction used for photocurrent mapping. Scale bar, 5 μm. (b) Photocurrent mapping of the p−n heterojunction under 0 V bias. The dashed lines outline the heterojunction regions. The solid lines outline the metal contacts. Contacts A and B are electrically connected to black phosphorus and MoS_2, respectively.

phosphorus/MoS_2 heterojunction to be used as large area transparent and flexible solar cells, as well as photodetectors.

CONCLUSION

In conclusion, for the first time, we demonstrate a gate-tunable black phosphorus−monolayer MoS_2 van der Waals heterojunction p−n diode. These 2D p−n diodes exhibit strong gate-tunable current-rectifying *I*−*V* characteristics, which is investigated using a simplified device model. As a photodetector, the p−n diode shows a photodetection responsivity of 418 mA/W, which is nearly 100 times higher than the reported black phosphorus phototransistor. Due to the small band gap and high mobility of few-layer black phosphorus, it is very suitable for broad-band and sensitive photodetection. Our p−n diodes also show photovoltaic power generation with a peak external quantum efficiency of 0.3%, which can be further improved by reducing the thickness of black phosphorus. Furthermore, photocurrent mapping is performed to study the spatial distribution of photoresponse, which reveals the importance of large area transparent electrodes for 2D p−n diodes to achieve large area optoelectronics applications.

METHODS

First, monolayer MoS_2 was synthesized using chemical vapor deposition method on heavily doped silicon wafer capping with 285 nm SiO_2. The black phosphorus was mechanically exfoliated from the bulk black phosphorus onto the wafer. The black phosphorus−monolayer MoS_2 heterojunction was achieved through the van der Waals interactions. Then the standard e-beam lithography process was used to define contact patterns and pads. A 20/60 nm Ni/Au was deposited as metal contacts. The electrical measurements were performed using Keithley 4200 semiconductor characterization system. All the electrical and optical measurements were performed in the ambient atmosphere.

Conflict of Interest: The authors declare no competing financial interest.

Acknowledgment. We thank Prof. Jong-Hyun Choi, Haorong Chen, and Te-Wei Wen from Purdue University for help with AFM characterization. This material is based upon work partly supported by NSF under Grant CMMI-1120577 and SRC under Task 2396.

Supporting Information Available: *I*−*V* characteristics of various devices, analysis of current transport in these p−n didoes, photodetection responsivity of a p−n diode, and thickness data of the few-layer black phosphorus flake for photocurrent mapping measurements. This material is available free of charge *via* the Internet at http://pubs.acs.org.

REFERENCES AND NOTES

1. Geim, A. K.; Novoselov, K. S. The Rise of Graphene. *Nat. Mater.* **2007**, *6*, 183–191.
2. Zhang, Y.; Tan, Y.-W.; Stormer, H. L.; Kim, P. Experimental Observation of the Quantum Hall Effect and Berry's Phase in Graphene. *Nature* **2005**, *438*, 201–204.
3. Geim, A. K. Graphene: Status and Prospects. *Science* **2009**, *324*, 1530–1534.
4. Novoselov, K. S.; Fal'ko, V. I.; Colombo, L.; Gellert, P. R.; Schwab, M. G.; Kim, K. A Roadmap for Graphene. *Nature* **2012**, *490*, 192–200.
5. Novoselov, K.; Jiang, D.; Schedin, F.; Booth, T.; Khotkevich, V.; Morozov, S.; Geim, A. Two-Dimensional Atomic Crystals. *Proc. Natl. Acad. Sci. U.S.A.* **2005**, *102*, 12451–10453.
6. Xu, M.; Liang, T.; Shi, M.; Chen, H. Graphene-like Two-Dimensional Materials. *Chem. Rev.* **2013**, *113*, 3766–3798.
7. Butler, S.; Hollen, S.; Cao, L.; Cui, Y.; Gupta, J.; Gutierrez, H.; Heinz, T.; Hong, S.; Huang, K.; Ismach, A.; *et al.* Progress, Challenges, and Opportunities in Two-Dimensional Materials beyond Graphene. *ACS Nano* **2013**, *7*, 2898–2926.
8. Wang, Q. H.; Kalantar-Zadeh, K.; Kis, A.; Coleman, J. N.; Strano, M. S. Electronics and Optoelectronics of Two-Dimensional Transition Metal Dichalcogenides. *Nat. Nanotechnol.* **2012**, *7*, 699–712.
9. Jariwala, D.; Sangwan, V. K.; Lauhon, L. J.; Marks, T. J.; Hersam, M. C. Emerging Device Applications for Semiconducting Two-Dimensional Transition Metal Dichalcogenides. *ACS Nano* **2014**, *8*, 1102–1120.
10. Radisavljevic, B.; Radenovic, A.; Brivio, J.; Giacometti, V.; Kis, A. Single-Layer MoS_2 Transistors. *Nat. Nanotechnol.* **2011**, *6*, 147–150.
11. Liu, H.; Neal, A. T.; Ye, P. D. Channel Length Scaling of MoS_2 MOSFETs. *ACS Nano* **2012**, *6*, 8563–8569.
12. Liu, H.; Neal, A. T.; Zhu, Z.; Luo, Z.; Xu, X.; Tománek, D.; Ye, P. D. Phosphorene: An Unexplored 2D Semiconductor with a High Hole Mobility. *ACS Nano* **2014**, *8*, 4033–4041.
13. Li, L.; Yu, Y.; Ye, G. J.; Ge, Q.; Ou, X.; Wu, H.; Feng, D.; Chen, X. H.; Zhang, Y. Black Phosphorus Field-Effect Transistors. *Nat. Nanotechnol.* **2014**, *9*, 372–377.
14. Morita, A. Semiconducting Black Phosphorus. *Appl. Phys. A: Solids Surf.* **1986**, *39*, 227–242.
15. Warschauer, D. Electrical and Optical Properties of Crystalline Black Phosphorus. *J. Appl. Phys.* **1963**, *34*, 1853–1860.
16. Bridgman, P. M. Two New Modifications of Phosphorus. *J. Am. Chem. Soc.* **1914**, *36*, 1344–1363.
17. Keyes, R. W. The Electrical Properties of Black Phosphorus. *Phys. Rev.* **1953**, *92*, 580–584.
18. Xia, F.; Wang, H.; Jia, Y. R. Rediscovering Black Phosphorus: A Unique Anisotropic 2D Material for Optoelectronics and Electronics. http://arxiv.org/abs/1402.0270, **2014**.
19. Buscema, M.; Groenendijk, D. J.; Blanter, S. I.; Steele, G. A.; Der, H. S. J. Van Castellanos-Gomez, A. Fast and Broadband Photoresponse of Few-Layer Black Phosphorus Field-Effect Transistors. http://arxiv.org/abs/1403.0565, **2014**.
20. Koenig, S. P.; Doganov, R. A.; Schmidt, H.; Neto, A. H.; Oezyilmaz, B. Electric Field Effect in Ultrathin Black Phosphorus. *Appl. Phys. Lett.* **2014**, *104*, 103106.
21. Yu, W. J.; Li, Z.; Zhou, H.; Chen, Y.; Wang, Y.; Huang, Y.; Duan, X. Vertically Stacked Multi-heterostructures of Layered Materials for Logic Transistors and Complementary Inverters. *Nat. Mater.* **2013**, *12*, 246–252.
22. Yang, H.; Heo, J.; Park, S.; Song, H. J.; Seo, D. H.; Byun, K.-E.; Kim, P.; Yoo, I.; Chung, H.-J.; Kim, K. Graphene Barristor, a Triode Device with a Gate-Controlled Schottky Barrier. *Science* **2012**, *336*, 1140–1143.
23. Britnell, L.; Gorbachev, R. V.; Jalil, R.; Belle, B. D.; Schedin, F.; Mishchenko, A.; Georgiou, T.; Katsnelson, M. I.; Eaves, L.; Morozov, S. V.; *et al.* Field-Effect Tunneling Transistor Based on Vertical Graphene Heterostructures. *Science* **2012**, *335*, 947–950.
24. Britnell, L.; Ribeiro, R. M.; Eckmann, A.; Jalil, R.; Belle, B. D.; Mishchenko, A.; Kim, Y.-J.; Gorbachev, R. V.; Georgiou, T.; Morozov, S. V.; *et al.* Strong Light−Matter Interactions in Heterostructures of Atomically Thin Films. *Science* **2013**, *340*, 1311–1314.
25. Yu, W. J.; Liu, Y.; Zhou, H.; Yin, A.; Li, Z.; Huang, Y.; Duan, X. Highly Efficient Gate-Tunable Photocurrent Generation in Vertical Heterostructures of Layered Materials. *Nat. Nanotechnol.* **2013**, *8*, 952–958.
26. Bertolazzi, S.; Krasnozhon, D.; Kis, A. Nonvolatile Memory Cells Based on MoS_2/Graphene Heterostructures. *ACS Nano* **2013**, 3246–3252.
27. Georgiou, T.; Jalil, R.; Belle, B. D.; Britnell, L.; Gorbachev, R. V.; Morozov, S. V.; Kim, Y.-J.; Gholinia, A.; Haigh, S. J.; Makarovsky, O.; *et al.* Vertical Field-Effect Transistor Based on Graphene-WS_2 Heterostructures for Glexible and Transparent Electronics. *Nat. Nanotechnol.* **2013**, *8*, 100–103.
28. Fang, H.; Battaglia, C.; Carraro, C.; Nemsak, S.; Ozdol, B.; Kang, J. S.; Bechtel, H. A.; Desai, S. B.; Kronast, F.; Unal, A. A.; *et al.* Strong Interlayer Coupling in van der Waals Heterostructures Built from Single-Layer Chalcogenides. *Proc. Natl. Acad. Sci. U.S.A.* **2014**, 10.1073/pnas.1405435111.
29. Lee, C.; Lee, G.; Van Der Zande, A. M.; Chen, W.; Li, Y.; Han, M.; Cui, X.; Arefe, G.; Nuckolls, C.; Heinz, T. F.; *et al.* Atomically Thin p-n Junctions with van der Waals Heterointerfaces. http://xxx.tau.ac.il/abs/1403.3062, **2014**.
30. Furchi, M. M.; Pospischil, A.; Libisch, F.; Burgdörfer, J.; Mueller, T. Photovoltaic Effect in an Electrically Tunable van der Waals Heterojunction. http://arxiv.org/abs/1403.2652, **2014**.

31. Cheng, R.; Li, D.; Zhou, H.; Wang, C.; Yin, A.; Jiang, S.; Liu, Y.; Chen, Y.; Huang, Y.; Duan, X. Electroluminescence and Photocurrent Generation from Atomically Sharp WSe_2/MoS_2 Heterojunction p-n Diodes. http://arxiv.org/abs/1403.3447, **2014**.
32. Jariwala, D.; Sangwan, V. K.; Wu, C.-C.; Prabhumirashi, P. L.; Geier, M. L.; Marks, T. J.; Lauhon, L. J.; Hersam, M. C. Gate-Tunable Carbon Nanotube-MoS_2 Heterojunction p-n Diode. *Proc. Natl. Acad. Sci. U.S.A.* **2013**, *110*, 18076–18080.
33. Chuang, S.; Kapadia, R.; Fang, H.; Chia Chang, T.; Yen, W.-C.; Chueh, Y.-L.; Javey, A. Near-Ideal Electrical Properties of InAs/WSe_2 van der Waals Heterojunction Diodes. *Appl. Phys. Lett.* **2013**, *102*, 242101.
34. Lam, K.; Cao, X.; Guo, J. Device Performance of Heterojunction Tunneling Field-Effect Transistors Based on Transition Metal Dichalcogenide Monolayer. *IEEE Electron Device Lett.* **2013**, *34*, 1331–1333.
35. Baugher, B. W. H.; Churchill, H. O. H.; Yang, Y.; Jarillo-Herrero, P. Optoelectronic Devices Based on Electrically Tunable p-n Diodes in a Monolayer Dichalcogenide. *Nat. Nanotechnol.* **2014**, *9*, 262–267.
36. Pospischil, A.; Furchi, M. M.; Mueller, T. Solar-Energy Conversion and Light Emission in an Atomic Monolayer p-n Diode. *Nat. Nanotechnol.* **2014**, *9*, 257–261.
37. Najmaei, S.; Liu, Z.; Zhou, W.; Zou, X.; Shi, G.; Lei, S.; Yakobson, B. I.; Idrobo, J.-C.; Ajayan, P. M.; Lou, J. Vapour Phase Growth and Grain Boundary Structure of Molybdenum Disulphide Atomic Layers. *Nat. Mater.* **2013**, *12*, 754–759.
38. Liu, H.; Si, M.; Deng, Y.; Neal, A. T.; Du, Y.; Najmaei, S.; Ajayan, P. M.; Lou, J.; Ye, P. D. Switching Mechanism in Single-Layer Molybdenum Disulfide Transistors: An Insight into Current Flow across Schottky Barriers. *ACS Nano* **2013**, *8*, 1031–1038.
39. Splendiani, A.; Sun, L.; Zhang, Y.; Li, T.; Kim, J.; Chim, C.-Y.; Galli, G.; Wang, F. Emerging Photoluminescence in Monolayer MoS_2. *Nano Lett.* **2010**, *10*, 1271–1275.
40. Liu, H.; Si, M.; Najmaei, S.; Neal, A.; Du, Y.; Ajayan, P.; Lou, J.; Ye, P. D. Statistical Study of Deep Submicron Dual-Gated Field-Effect Transistors on Monolayer Chemical Vapor Deposition Molybdenum Disulfide Films. *Nano Lett.* **2013**, *13*, 2640–2646.
41. Lopez-Sanchez, O.; Lembke, D.; Kayci, M.; Radenovic, A.; Kis, A. Ultrasensitive Photodetectors Based on Monolayer MoS_2. *Nat. Nanotechnol.* **2013**, *8*, 497–501.
42. Dai, J.; Zeng, X. Bilayer Phosphorene: Effect of Stacking Order on Bandgap and Its Potential Application in Thin-Film Solar Cells. *J. Phys. Chem. Lett.* **2014**, *5*, 1289–1293.
43. Du, Y.; Yang, L. M.; Zhang, J. Y.; Liu, H.; Majumdar, K.; Kirsch, P. D.; Ye, P. D. MoS_2 Field-Effect Transistors with Graphene/Metal Heterocontacts. *IEEE Electron Device Lett.* **2014**, *5*, 599–601.